Low-lying vibronic level structure of the ground state of the methoxy radical: Slow electron velocity-map imaging (SEVI) spectra and Köppel-Domcke-Cederbaum (KDC) vibronic Hamiltonian calculations

Marissa L. Weichman, Lan Cheng, Jongjin B. Kim, John F. Stanton, and Daniel M. Neumark

Citation: The Journal of Chemical Physics **146**, 224309 (2017); doi: 10.1063/1.4984963
View online: http://dx.doi.org/10.1063/1.4984963
View Table of Contents: http://aip.scitation.org/toc/jcp/146/22
Published by the American Institute of Physics

Low-lying vibronic level structure of the ground state of the methoxy radical: Slow electron velocity-map imaging (SEVI) spectra and Köppel-Domcke-Cederbaum (KDC) vibronic Hamiltonian calculations

Marissa L. Weichman,[1] Lan Cheng,[2] Jongjin B. Kim,[1,a)] John F. Stanton,[3,b)] and Daniel M. Neumark[1,4,b)]

[1]*Department of Chemistry, University of California, Berkeley, California 94720, USA*
[2]*Department of Chemistry, The Johns Hopkins University, Baltimore, Maryland 21208, USA*
[3]*Quantum Theory Project, Department of Chemistry and Physics, University of Florida, Gainesville, Florida 32611, USA*
[4]*Chemical Sciences Division, Lawrence Berkeley National Laboratory, Berkeley, California 94720, USA*

(Received 31 March 2017; accepted 23 May 2017; published online 12 June 2017)

A joint experimental and theoretical study is reported on the low-lying vibronic level structure of the ground state of the methoxy radical using slow photoelectron velocity-map imaging spectroscopy of cryogenically cooled, mass-selected anions (cryo-SEVI) and Köppel-Domcke-Cederbaum (KDC) vibronic Hamiltonian calculations. The KDC vibronic model Hamiltonian in the present study was parametrized using high-level quantum chemistry, allowing the assignment of the cryo-SEVI spectra for vibronic levels of CH_3O up to 2000 cm^{-1} and of CD_3O up to 1500 cm^{-1} above the vibrational origin, using calculated vibronic wave functions. The adiabatic electron affinities of CH_3O and CD_3O are determined from the cryo-SEVI spectra to be 1.5689 ± 0.0007 eV and 1.5548 ± 0.0007 eV, respectively, demonstrating improved precision compared to previous work. Experimental peak splittings of <10 cm^{-1} are resolved between the $e_{1/2}$ and $e_{3/2}$ components of the 6_1 and 5_1 vibronic levels. A pair of spin-vibronic levels at 1638 and 1677 cm^{-1} were predicted in the calculation as the $e_{1/2}$ and $e_{3/2}$ components of 6_2 levels and experimentally resolved for the first time. The strong variation of the spin-orbit splittings with a vibrational quantum number is in excellent agreement between theory and experiment. The observation of signals from nominally forbidden a_1 vibronic levels in the cryo-SEVI spectra also provides direct evidence of vibronic coupling between ground and electronically excited states of methoxy. *Published by AIP Publishing.* [http://dx.doi.org/10.1063/1.4984963]

I. INTRODUCTION

The methoxy radical (CH_3O) is one of the most fundamental and important transient intermediates in all of chemistry. In addition to playing an important role in the initial stages of methane combustion,[1] CH_3O is also involved in atmospheric processes;[2] after OH radicals abstract a hydrogen atom from methane, the reaction of CH_3 with O_2 produces the collisionally stabilized methyl peroxyl radical, which can subsequently be converted to methoxy and NO_2 when it encounters NO.[3] This process ultimately produces formaldehyde and HO_2 when methoxy reacts with atmospheric O_2. In addition, CH_3O is the parent compound for all alkoxy radicals, which are a ubiquitous class of reactive intermediates featured in atmospheric chemistry,[4] combustion,[5] radiolysis,[6] and organic photochemistry.[7]

Alkoxy radicals are also of significant interest to theoreticians due to their lowest degenerate (or nearly degenerate) electronic states. Methoxy is one of the simplest molecules to exhibit the Jahn-Teller (JT) effect, and as such has been the subject of a great deal of study over the years. In C_{3v} symmetry, its ground electronic state has ^2E symmetry, and the molecule distorts to an equilibrium structure that has C_s symmetry. On the lowest adiabatic and nonrelativistic potential energy surface, the stabilized geometry is one in which the C–O bond—which lies along the C_3 rotation axis in the C_{3v} structure—is bent towards the bisector of the two equivalent C–H bonds. The magnitude of this stabilization, however, is quite small both in terms of energy and geometry; the JT effect in CH_3O is quite weak.[8] Partly because of this, the spin-orbit (SO) effect—which is often largely or completely quenched in open-shell molecules with moderate to strong JT effects—is prominent in CH_3O, where splitting of the ground vibronic e state is roughly 60 cm^{-1}. In substituted methoxy radicals, the three-fold axis of symmetry is generally broken, and the exact spatial degeneracy and consequent JT effect are replaced by a very small splitting between the ground and first excited electronic states,[9] which can be discussed and analyzed in terms of the pseudo-JT effect.

First detected in the fluorescence spectrum of ethyl nitrate vapor,[10] spectroscopic studies of the methoxy ground state[11] have been largely based on electronic spectroscopy although there is a notable and very recent infrared study.[12] The $\tilde{A}^2A_1$

a)Present address: Stanford Linear Accelerator Center (SLAC) National Accelerator Laboratory, Menlo Park, CA 94025, USA.
b)Authors to whom correspondence should be addressed: johnstanton@ufl.edu and dneumark@berkeley.edu.

state lies roughly 4 eV above the electronic ground state, and the $\tilde{A} \leftarrow \tilde{X}$ electronic transition is quite strong. While it also provides an avenue for exploring excited state dynamics of methoxy,[13] the $\tilde{A} \leftarrow \tilde{X}$ electronic transition has been exploited to study the vibronic structure of the ground state using stimulated emission pumping (SEP)[14,15] as well as laser-induced and dispersed fluorescence (LIF and DF).[16–20] Studies of CH_3O by the latter techniques have been brought to a quite mature state by Miller and co-workers, as LIF spectra revealing both the ground vibronic level and its spin-orbit partner have been recorded with rotational resolution.[17] Accordingly, much is now understood about the vibrational levels in the ground state, but the fact that both JT and SO effects are operative in CH_3O renders the spectra complicated and assignments difficult. Above 2000 cm^{-1}, the spectra remain very difficult to interpret in terms of conventional assignments.

Another approach to the spectroscopic investigation of CH_3O comes from negative ion photoelectron spectroscopy of the quite stable closed-shell methoxide anion, CH_3O^-. The first such study used a traditional fixed-wavelength photon source and lacked sufficient resolution to observe any of the subtle vibronic and spin-orbit features that are present in the vibronic energy level structure of this small and quite complicated molecule.[21] Subsequent work with higher resolution but still fixed-wavelength sources was able to see spin-orbit splitting of the ground state indirectly through a conspicuously broadened band.[22,23] These spectra present strong evidence for Jahn-Teller effects, as they are not dominated by progressions in totally symmetric modes. Given the magnitude of the splitting in methoxy, traditional photoelectron spectroscopy—which typically has 50–100 cm^{-1} resolution—is not sufficient. Consequently, methoxy was one of the first molecules studied with the higher-resolution slow photoelectron velocity-map imaging (SEVI) technique.[24] SEVI uses tunable photodetachment laser wavelengths so that the energy levels of interest can be probed with very low kinetic energy photoelectrons, leading to sub-millielectronvolt energy resolution. Using this technique, Nee *et al.* obtained the first photoelectron spectrum to resolve spin-orbit levels in CH_3O.[25] Together with a number of hot bands and sequence bands, this study provided a rich source of information about the vibrational levels of both CH_3O and its anion, as well as the electron affinity (1.5690 ± 0.0019 and 1.5546 ± 0.0019 eV for CH_3O and CD_3O, respectively). In that work, the *e* vibronic components of CH_3O were observed for all normal modes except the totally symmetric C–H stretch, and spin-orbit components were seen directly for both the origin band (splitting reported as 63 cm^{-1}) and the ν_2 umbrella mode (53 cm^{-1}).

Although several notable and high-quality theoretical studies of methoxy have been reported,[26,27] the most elaborate investigations of the ground state are those carried out by Shao and Mo[28] and by Sibert and co-workers[12] using a quasidiabatic representation[29,30] parametrized by calculations carried out at the CCSD(T)[31] level of theory with correlation-consistent basis sets.[32] In particular, in the recent study of the matrix isolated infrared spectrum,[12] the vibrational assignments were facilitated by use of a model Hamiltonian whose eigenvectors can be inspected to reveal the quantum numbers and angular momentum of the states, to the degree that the former can be deduced. Analysis of the rather complex and congested matrix spectrum provided a reasonably complete assignment of all levels that are predicted to lie below 1700 cm^{-1}; only the upper spin-orbit component of the C–O stretching mode (ν_3) was not observed.

In this work, we report SEVI spectra of CH_3O that exhibit markedly better resolution than those of the previous study,[25] together with high-level vibronic calculations parametrized by sophisticated electronic structure calculations. The spectra have been obtained with cryogenic cooling of the mass-selected anions (cryo-SEVI),[33] thereby removing all interference from hot bands and sequence bands. In addition, due to improvements of the SEVI instrument since the first pioneering study, more spin-orbit splittings of *e* vibronic levels have been resolved, two with magnitudes of less than 10 cm^{-1}. Many of the band positions reported here are more precise than those determined from earlier DF measurements (due to resolution issues) and are also not affected by interactions of the molecule with a matrix substrate. Moreover, we report a band that has apparently not been previously observed and provide direct evidence of vibronic coupling linking the ground state of CH_3O with the excited $\tilde{A}^2A_1$ electronic state.

II. METHODS

A. Experimental techniques

The cryo-SEVI method and apparatus have been described in detail elsewhere.[24,33,34] In brief, cryogenically cooled, mass-selected anions are photodetached with a tunable laser. The electron kinetic energy (eKE) distribution of the resulting photoelectrons is measured with a velocity-map imaging (VMI) spectrometer. The spectrometer has a roughly constant resolving power ΔeKE/eKE, resulting in the best resolution for imaging low-eKE electrons. Low extraction voltages are used to magnify the image of the slowest electrons on the detector, yielding instrumental energy resolution down to 1 cm^{-1} with the current configuration of the VMI lens.[34]

Methoxide anions are prepared by expanding a dilute gas mixture of methanol and NF_3 in helium buffer gas through a pulsed Even-Lavie solenoid valve[35] fitted with a circular filament ionizer. Electrons from the ionizer induce dissociative attachment of NF_3, producing F^- which then deprotonates methanol to form the desired methoxide anions. The anions are directed through a radiofrequency (RF) hexapole ion guide and a quadrupole mass filter, and into a linear RF octupole ion trap. The trap is held at 5 K and filled with pulses of an 80:20 He:H_2 buffer gas mixture. The ions are stored for ~40 ms, enabling collisional cooling to their ground vibrational and electronic states.[33] The cold ions are then extracted from the trap into an orthogonal time-of-flight mass spectrometer. After mass selection, the anions reach the interaction region where they are photodetached with the output of an Nd:YAG-pumped dye laser. The resulting photoelectrons are focused by the VMI electrostatic lens[36] onto a detector comprising

two chevron-stacked microchannel plates (MCPs) coupled to a phosphor screen;[37] events on the screen are recorded with a CCD camera.

During data acquisition, an event counting algorithm identifies single electron events and computes their centroids.[38] The maximum-entropy velocity Legendre reconstruction method[39] is then used to reconstruct the radial and angular electron distributions from the accumulated image. The velocity (and hence eKE) of the photoelectrons is calibrated as a function of radial displacement using SEVI images of O^- atomic anions[40] taken at many photon energies. As the eKE depends on the photodetachment laser energy ($h\nu$), SEVI spectra are plotted in electron binding energy (eBE), given by eBE = $h\nu$ − eKE.

SEVI spectra are acquired at discrete photodetachment energies tuned just above spectral features of interest. The low-eKE windows of these spectra are spliced together to create a composite high-resolution spectrum of the full region. In the composite trace, the intensity of a given feature is scaled to the intensity of that feature in a low-resolution overview spectrum to minimize threshold effects that may distort relative peak intensities.

B. Computational aspects

The calculations presented here target vibronic levels of methoxy within its electronic ground state. For this purpose, a two-state diabatic Hamiltonian[29,30] has been adopted

$$H^{dia} = \begin{pmatrix} T_N^{AA} & 0 \\ 0 & T_N^{BB} \end{pmatrix} + \begin{pmatrix} V^{AA} & V^{AB} \\ V^{BA} & V^{BB} \end{pmatrix} + \begin{pmatrix} 0 & iA^{SO} \\ -iA^{SO} & 0 \end{pmatrix}, \quad (1)$$

expressed in the basis of diabatic electronic states described by wave functions ψ_A and ψ_B, which are the two components of the degenerate electronic ground state of methoxy. In our calculations, real-valued basis functions are used for both electronic and vibrational states, and ψ_A and ψ_B are chosen to transform as A' and A'' irreducible representations in the C_s point group. Exploratory calculations indicate that the excited electronic $\tilde{A}^2A_1$ state, lying more than 30 000 cm^{-1} above the ground vibronic level, has a negligible influence on the vibronic level positions targeted in the present work. Therefore the $\tilde{A}^2A_1$ state is not considered in the present calculations of the vibronic energy levels. On the other hand, coupling between the ground and $\tilde{A}^2A_1$ states is responsible for the appearance of the a_1 vibronic levels that are observed here as well as in previous studies of the photodetachment of methoxide and calculations using a three-state Hamiltonian will be of interest for future studies on the intensities of these "symmetry forbidden" levels.

The nuclear kinetic energy operator is assumed block diagonal in the (quasi)diabatic representation. The diabatic potential V is determined from adiabatic energies obtained from quantum-chemical calculations. In our parameterization of the potential, the reference geometry has been chosen as the minimum of the conical intersection seam optimized at the equation-of-motion ionization potential coupled cluster singles and doubles (EOMIP-CCSD) level[41] with atomic natural orbital (ANO) basis sets[42] of double-zeta quality (ANO0). The potential energy has been expanded in a Taylor series up to the fourth order with respect to normal coordinates obtained from CCSD/ANO0 calculations of methoxide at the reference geometry. The quality of the linear and quadratic force constants is of crucial importance in the accurate determination of level positions, but it is in general sufficient to augment the high-quality linear and quadratic force constants with anharmonic force constants obtained at a lower level of theory. Therefore, the linear and quadratic force constants have been calculated using the highly accurate EOMIP-CC singles, doubles, and triples (EOMIP-CCSDT) method[43] with ANO basis sets of triple-zeta quality (ANO1), while the cubic and quartic force constants have been computed at the more approximate EOMIP-CCSD/ANO0 level. Cubic and quartic force constants with labels from three different JT modes are approximated as the corresponding force constants of methoxide. This is expected to be a good approximation since the JT effect in higher orders is expected to be very small and the diabatic anion constants should be close to those of the neutral.

Due to the use of the real-valued electronic basis functions, the spin-orbit coupling parameter appears on the off-diagonal block of the diabatic Hamiltonian

$$iA^{SO} = \langle \psi_A | \hat{h}_z^{SO} | \psi_B \rangle. \quad (2)$$

We have adopted a value of −66.5 cm^{-1} for A^{SO} calculated at the reference geometry using degenerate perturbation theory with EOMIP-CCSD wave functions[44] and the ANO1 basis. The effective one-electron spin-orbit operator has been constructed using the molecular mean-field approach.[45] This value of A^{SO} is treated as geometry-independent in our calculation, as is consistent with the use of the Condon approximation in calculations of this type. The geometry-independent A^{SO} has nonzero matrix elements between vibronic functions of different rows of e irreducible representation and also between a_1 and a_2 functions. Therefore the e states, which are doubly degenerate in the absence of spin-orbit coupling, are split into $e_{1/2}$ and $e_{3/2}$ states. The a_1 and a_2 solutions in the non-relativistic case are also coupled together by A^{SO}, while one could still assign some low-lying vibronic levels to a_1 or a_2 according to the symmetry of the dominating contribution.

After constructing the diabatic Hamiltonian, the nuclear Schrödinger equation has been solved variationally using the Lanczos algorithm to obtain the vibronic levels and wave functions. In this two-state scheme, the vibronic wave function (Ψ_c) is expanded as

$$\Psi_c = \psi_A \phi_c^A + \psi_B \phi_c^B, \quad (3)$$

$$\phi_c^A = \sum_m C_{mc}^A \eta_m \ , \ \phi_c^B = \sum_m C_{mc}^B \eta_m, \quad (4)$$

where η_m are the vibrational basis functions and C_{mA} and C_{mB} are the corresponding expansion coefficients [elements of the eigenvectors of the Hamiltonian given by Eq. (1)]. Following the standard procedure, η_m are chosen as the direct product of harmonic oscillator functions of the nine normal modes, i.e.,

$$\begin{aligned} \{\eta_m &= \eta_{(n_1,n_2,n_3,n_{4a},n_{4b},n_{5a},n_{5b},n_{6a},n_{6b})} \\ &= \chi^1_{(n_1)}\chi^2_{(n_2)}\chi^3_{(n_3)}\chi^{4a}_{(n_{4a})}\chi^{4b}_{(n_{4b})}\chi^{5a}_{(n_{5a})}\chi^{5b}_{(n_{5b})}\chi^{6a}_{(n_{6a})}\chi^{6b}_{(n_{6b})} \\ n_i &= 0, 1, \ldots, n_i^{max} \Big\} . \end{aligned}$$

TABLE I. Vibrational modes of the methoxy radical.

	Mode	Symmetry
1	C–H symmetric stretching	a_1
2	Umbrella	a_1
3	C–O stretching	a_1
4	C–H antisymmetric stretching	e
5	Scissoring	e
6	Rocking	e

The vibrational modes of methoxy are summarized in Table I. The nondegenerate modes 1, 2, and 3 represent the C–H symmetric stretching mode, the umbrella mode, and the C–O stretching mode, respectively, while the degenerate modes 4, 5, and 6 correspond to the C–H asymmetric stretching mode, the scissoring mode, and the rocking mode, respectively. In the calculation of CH_3O, the maximum quantum numbers in the basis have been chosen as

$$(n_1^{max}, n_2^{max}, n_3^{max}, n_{4a}^{max}, n_{4b}^{max}, n_{5a}^{max}, n_{5b}^{max}, n_{6a}^{max}, n_{6b}^{max}) = (5, 6, 6, 5, 5, 6, 6, 9, 9), \quad (5)$$

and 3000 iterations have been used in the Lanczos diagonalization procedure. With this option of basis sets and number of iterations, all the vibronic levels up to 2000 cm^{-1} are converged to within 1 cm^{-1}. Those between 2000 cm^{-1} and 2500 cm^{-1} are converged to within 3 cm^{-1}. In the calculation of CD_3O presented here, the maximum quantum numbers in the basis have been chosen as

$$(n_1^{max}, n_2^{max}, n_3^{max}, n_{4a}^{max}, n_{4b}^{max}, n_{5a}^{max}, n_{5b}^{max}, n_{6a}^{max}, n_{6b}^{max}) = (4, 7, 7, 4, 4, 7, 7, 8, 8), \quad (6)$$

again together with 3000 iterations in the Lanczos diagonalization procedure. All vibronic levels up to 1500 cm^{-1} are converged to within 1 cm^{-1}, while those between 1500 cm^{-1} and 2000 cm^{-1} are converged to within 3 cm^{-1}.

The intensity for a transition to the vibronic state Ψ_c in the photoelectron spectrum can then be written as

$$I_c = |\langle \Psi_{gr}^{anion} | \hat{O}_{dipole} | \Psi_c \otimes \Psi^e \rangle|^2, \quad (7)$$

where Ψ_{gr}^{anion} is the wave function for the vibronic ground state of the anion and Ψ^e is the wave function of the free electron ejected during the photoelectron process. As the anion is a well-behaved closed-shell molecule, Ψ_{gr}^{anion} can be accurately represented within the adiabatic approximation

$$\Psi_{gr}^{anion} = \psi^{anion} \phi_{gr}^{anion}. \quad (8)$$

Within the Condon approximation, the expression for the intensities can be approximated as the product of an electronic and a vibrational contribution

$$I_c \approx T_{dipole} T_{vib}, \quad (9)$$

$$T_{dipole} = |\langle \psi^{anion} | \hat{O}_{dipole} | \psi^A \otimes \psi^e \rangle|^2 = |\langle \psi^{anion} | \hat{O}_{dipole} | \psi^B \otimes \psi^e \rangle|^2, \quad (10)$$

$$T_{vib} = |\langle \phi_{gr}^{anion} | \phi_c^A \rangle|^2 + |\langle \phi_{gr}^{anion} | \phi_c^B \rangle|^2 = 2|\langle \phi_{gr}^{anion} | \phi_c^A \rangle|^2. \quad (11)$$

While T_{dipole} represents the electronic dipole transition matrix element, and T_{vib} is the overlap of vibrational wave functions and gives, to a good approximation, the relative intensities of the vibronic levels. Note that $\langle \phi_{gr}^{anion} | \phi_c^A \rangle = \pm i \langle \phi_{gr}^{anion} | \phi_c^B \rangle$ for $e_{3/2}$ and $e_{1/2}$ states, respectively. In order to directly obtain T_{vib} using the Lanczos algorithm without storing the wave functions, the vibrational ground state wave function of the anion, ϕ_{gr}^{anion}, has been used as the seed for the ϕ_c^A block in the solution of the nuclear Schrödinger equation. Then twice the square of the coefficient for the seed vector in the Lanczos (tridiagonal) basis gives T_{vib}.

III. RESULTS AND DISCUSSION

A. Experimental results

The experimental cryo-SEVI spectra of CH_3O and CD_3O, taken with an ion trap temperature of 5 K, are presented in Figs. 1 and 2, respectively. These spectra are consistent with the early SEVI results of Nee *et al.*[25] but are considerably cleaner and better resolved. The spectra of both species demonstrate a strong spin-orbit split vibrational origin (peaks *a* and *b*), with irregular higher-lying vibrational structure continuing for a few thousand wavenumbers. Positions and assignments of the peaks labeled in Figs. 1 and 2 are reported in Tables II and III, and are compared to theoretical and experimental literature values in Tables IV and V. The positions of the peaks represent the centers of Gaussian fits to the experimental data.

For both CH_3O and CD_3O, no spectroscopic features are observed lying below the peaks labeled *a* in eBE,

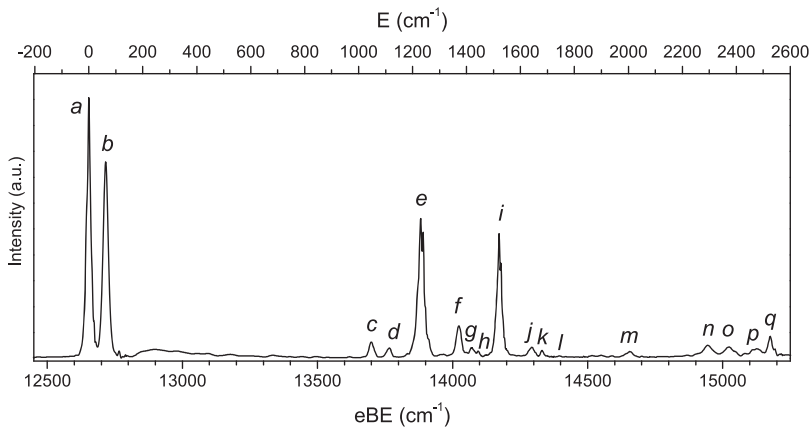

FIG. 1. Cryo-SEVI spectrum of CH_3O. The energy scale is shown in cm^{-1} for both electron binding energy (eBE) and energy relative to the vibrational origin (E).

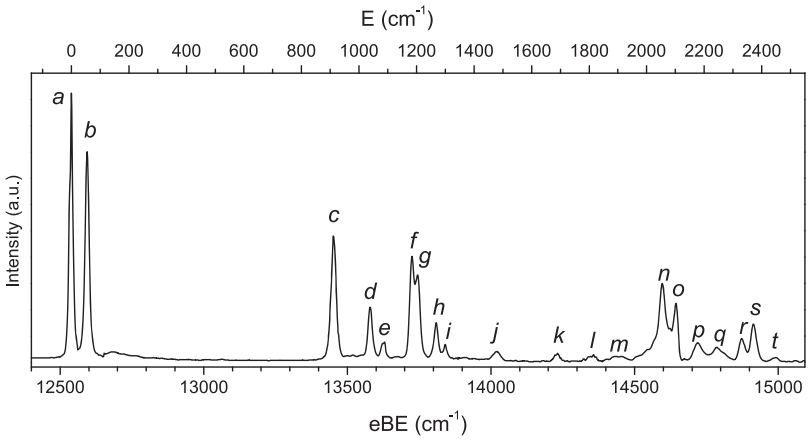

FIG. 2. Cryo-SEVI spectrum of CD_3O. The energy scale is shown in cm^{-1} for both electron binding energy (eBE) and energy relative to the vibrational origin (E).

indicating that vibrational hot bands and sequence bands present in the previous SEVI study[25] have been completely suppressed by cryogenic cooling. Cold anion rotational distributions lead to typical peak widths of 10 cm^{-1} fwhm in the cryo-SEVI spectra, compared to the 30–40 cm^{-1} fwhm typical of the original SEVI experiment. For CH_3O, narrow spin-orbit splittings of less than 10 cm^{-1} are resolved for peaks *e* and *i*.

All intense peaks in the cryo-SEVI spectra demonstrate photoelectron angular distributions enhanced perpendicular to the laser polarization axis, as was also reported by Ramond *et al.*[23] and by Nee *et al.*[25] This measured perpendicular anisotropy is consistent with detachment transitions of *e* vibronic character.[46]

B. Computed spectra and assignment for CH_3O

We first demonstrate the convergence of the calculated photoelectron spectrum with respect to the parametrization of the diabatic potential in the model Hamiltonian. In Fig. 3, the computational results obtained using a linear model, a quadratic model, a cubic model, and the final quartic model are presented (red stick spectra) and compared with the experimental spectrum (black). Obviously, the results obtained with the linear or quadratic models deviate substantially from the experiment and are not useful for the quantitative interpretation of the experimental results. The energy levels calculated with the linear model exhibit errors of more than 200 cm^{-1} even for the a_1 component of the 6_1 level; the energy levels up to 2000 cm^{-1} computed using the quadratic level are somewhat better but still typically in error by 50–100 cm^{-1}. This is perhaps not surprising as the use of a quadratic model, which is often appropriate and sufficient for interpreting infrared spectra of simple systems, is inadequate to treat the much more complex problem posed here involving both Jahn-Teller coupling and spin-orbit coupling. However, when the Hamiltonian is expanded through quartic terms, very good agreement is found with the observed level positions. Most of the energy levels calculated

TABLE II. Cryo-SEVI peak positions for CH_3O and assignments for features within 2000 cm^{-1} of the vibrational origin.

Feature	eBE (cm^{-1})	E (cm^{-1})	Assignment
a	12 654	0	0_0 ($e_{3/2}$)
b	12 716	62	0_0 ($e_{1/2}$)
c	13 699	1045	3_1 ($e_{3/2}$)
d	13 764	1110	3_1 ($e_{1/2}$)
e	13 882	1228	6_1 ($e_{1/2}$)
	13 891	1237	6_1 ($e_{3/2}$)
f	14 022	1368	2_1 ($e_{3/2}$)
g	14 070	1416	2_1 ($e_{1/2}$)
h	14 095	1441	5_1 (a_1)
i	14 172	1518	5_1 ($e_{1/2}$)
	14 178	1525	5_1 ($e_{3/2}$)
j	14 292	1638	6_2 ($e_{1/2}$)
k	14 331	1677	6_2 ($e_{3/2}$)
l	14 395	1741	3_16_1 (a_1)
m	14 654	2001	5_16_1 ($e_{3/2}$ and $e_{1/2}$)
n	14 946	2292	
o	15 023	2369	
p	15 125	2471	
q	15 176	2522	

TABLE III. Cryo-SEVI peak positions for CD_3O and assignments for features within 1500 cm^{-1} of the vibrational origin.

Feature	eBE (cm^{-1})	E (cm^{-1})	Assignment
a	12 539	0	0_0 ($e_{3/2}$)
b	12 594	55	0_0 ($e_{1/2}$)
c	13 451	912	$6_1 + 5_1$ ($e_{1/2}$), $6_1 + 3_1$ ($e_{3/2}$)
d	13 579	1040	3_1 ($e_{1/2}$), 2_1 ($e_{3/2}$)
e	13 627	1088	2_1 ($e_{1/2}$)
f	13 725	1186	$2_1 + 5_1 + 3_1$ ($e_{3/2}$)
g	13 744	1205	$2_1 + 5_1 + 3_1$ ($e_{1/2}$)
h	13 809	1270	6_2 ($e_{1/2}$)
i	13 841	1302	6_2 ($e_{3/2}$)
j	14 020	1481	5_16_1 ($e_{3/2}$ and $e_{1/2}$)
k	14 230	1691	
l	14 352	1813	
m	14 443	1905	
n	14 597	2059	
o	14 641	2103	
p	14 722	2183	
q	14 789	2250	
r	14 874	2336	
s	14 914	2376	
t	14 988	2450	

TABLE IV. Vibronic levels from 0 to 2000 cm^{-1} above the vibrational origin in the ground electronic state of CH_3O. Italicized values in the last column are the average of two features split by site effects in the matrix.

		Theory			Experiment			
Level	Symmetry	Reference 28	Reference 12	Present	SEVI	SEP	LIF	IR[12]
0_0	$e_{3/2}$	0	0	0	0	0	0	0
0_0	$e_{1/2}$	62	...	64	62	62[a]	62[b]	...
6_1	a_1	718	685	682	...	682[c]	685[d]	*692*
6_1	a_2	969	946	950	...	944	...	*949*
3_1	$e_{3/2}$	1046	1045	1041	1045	1045[a]	1047[d]	1042
3_1	$e_{1/2}$	1110	1107	1106	1110	1108[a]	1110[d]	...
6_1	$e_{1/2}$	1244	1222	1235	1228	1224	1230[d]	*1227*
6_1	$e_{3/2}$	1254	1233	1242	1237	1232	...	*1236*
5_1	a_2	1384	1344	1351	...	1344	...	1347
2_1	$e_{3/2}$	1382	1373	1356	1368	1365	1360[d]	1366
2_1	$e_{1/2}$	1430	1415	1396	1416	1413	1428[d]	1411
5_1	a_1	1465	1433	1436	1441	1433	...	1427
$2_1 + 5_1$	$e_{1/2}$	1533	1516	1503	1518	1517	1519[d]	1520
$5_1 + 2_1$	$e_{3/2}$	1547	1521	1509	1525	1523	...	1523
6_2	$e_{1/2}$	1681	1635	1630	1638	...	1652[d]	1651
6_2	$e_{3/2}$	1725	...	1674	1677	...	...	...
$3_1 6_1$	a_1	1788	1746	1739	1741	1746[c]	1745[d]	1780
$5_1 6_1$	$e_{3/2}$	2059	2009	2001	2001	...	...	1996
$5_1 6_1$	$e_{1/2}$	2061	2010	2001	2001	...	...	2001
$3_1 6_1$	a_2	2029	...	2003	...	...	...	...

[a]From Ref. 15.
[b]From Ref. 17.
[c]From Ref. 14.
[d]From Ref. 16.

to lie below 2000 cm^{-1} are within 10 cm^{-1} of the experiment with the largest deviation being 20 cm^{-1} for the $e_{1/2}$ component of the 2_1 state (peak *g* in Fig. 1), a level of accuracy comparable to that found in previous calculations of this type for the nitrate (NO_3) and formyloxyl (HCO_2) radicals.[47,48] We emphasize that this agreement is reached without any fitting of the experimental results. This finding is therefore congruent with the idea that contributions from anharmonic force fields are necessary

TABLE V. Vibronic levels from 0 to 1500 cm^{-1} above the vibrational origin in the ground electronic state of CD_3O. Italicized values in the last column are the average of two features split by site effects in the matrix.

		Theory			Experiment		
Level	Symmetry	Reference 28	Reference 12	Present	SEVI	LIF	IR[12]
0_0	$e_{3/2}$	0	0	0	0	0	0
0_0	$e_{1/2}$	55	...	57	55	55[a]	...
6_1	a_1	538	515	520	...	523[b]	*530*
6_1	a_2	741	721	730	...	734[b]	*730*
$6_1 + 5_1$	$e_{1/2}$	920	904	919	912	920[b]	912
$6_1 + 3_1$	$e_{3/2}$	925	913	926	912	948[b]	...
$5_1 + 6_1$	a_2	992	970	976	...	994[b]	974
3_1	$e_{3/2}$	1007	1005	1008	...	1015[b]	1006
3_1	$e_{1/2}$	1034	1036	1034	1040	1039[b]	1037
2_1	$e_{3/2}$	1063	1047	1038	1040	1087[b]	...
5_1	a_1	1064	1046	1052	...	1060[b]	...
2_1	$e_{1/2}$	1107	1087	1082	1088	...	...
$2_1 + 5_1 + 3_1$	$e_{3/2}$	1193	1180	1176	1186	1201[b]	1185
$2_1 + 5_1 + 3_1$	$e_{1/2}$	1214	1201	1201	1205	...	1224
6_2	$e_{1/2}$	1293	1261	1269	1270	...	1260
6_2	$e_{3/2}$	1328	1289	1303	1302	...	...
$5_1 6_1$	$e_{3/2}$	1514	1481	1485	1481	...	1481
$5_1 6_1$	$e_{1/2}$	1516	1482	1485	1481	...	1485
$3_1 6_1$	a_1	1508	1491	1496	...	...	1492

[a]From Ref. 18.
[b]From Ref. 16.

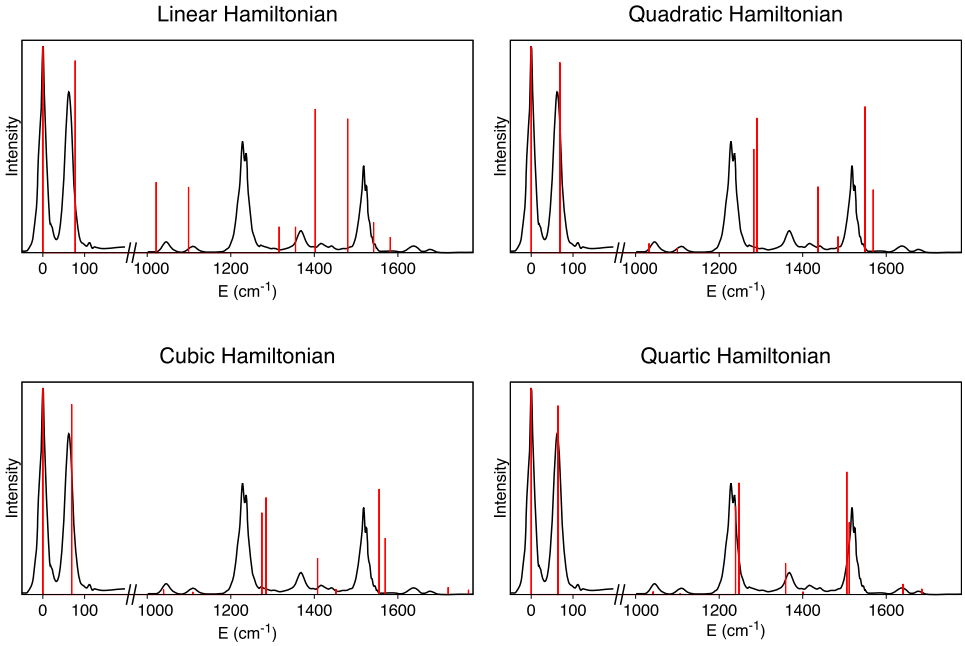

FIG. 3. Cryo-SEVI spectra of CH_3O (black) and simulated spectra using the KDC model Hamiltonian (red sticks). The maximum quantum number for basis functions in each mode is (3, 6, 6, 3, 3, 6, 6, 6, 6). Spectra are plotted in cm^{-1} relative to the position of the vibrational origin at 12 654 cm^{-1}.

for accurate calculations of level positions in vibronic systems and that cubic and quartic constants may be sufficient for these purposes.

Based on the calculations using the quartic Hamiltonian, the vibronic energy levels up to 2000 cm^{-1} are assigned to quantum numbers of certain vibrational modes, a task that is easily accomplished by establishing the symmetry of the states, inspecting the dominant contributions to the eigenvector, and, as needed, by inspecting the nodal properties of the corresponding vibronic eigenfunctions. The computed and observed energy levels of CH_3O are shown in the upper half of Fig. 4 and summarized along with the corresponding normal mode assignments in Table IV, where they are compared to previous experimental and computational values. The vibronic wave functions for most of the energy levels in this range are dominated by the contribution from one leading vibrational state and can thus be assigned to a (set of) vibrational quantum number(s). However, in this context, four of the levels warrant special mention. Specifically, the two at 1235 cm^{-1} and 1242 cm^{-1} that correspond to feature *e* in Fig. 1 have eigenvectors that exhibit appreciable mixing between the 6_1, 0_0, and 6_2 basis functions. It should be noted that the vibrational basis functions have been generated from the calculations of methoxide and thus are not expected to correspond perfectly to the vibrations of the methoxy radical due to Duschinsky mixing. Therefore, we retain the assignment of 6_1 for these two levels, as they belong to the first set of vibronic levels of the rocking mode (the mixing with 0_0 and 6_2 in the eigenvector here is due to the geometry change along the a' component of mode 6 being significant, or, equivalently, that the Franck-Condon activity of the mode is appreciable). Similarly, the levels at 1503 cm^{-1} and 1509 cm^{-1} (feature *i* in Fig. 1) can be assigned to 5_1 although the mixture of 2_1 in these two levels is pronounced.

Our computational and experimental results are in very good agreement with previous results, including the computational study of Shao and Mo[28] and the recent analysis of the IR spectrum by Sibert and co-workers.[12] We should mention that the spin-orbit components of the 6_2 combination level at 1638 cm^{-1} (peak *j* in Fig. 1) and 1677 cm^{-1} (peak *k* in Fig. 1) are experimentally resolved for the first time in the present work,

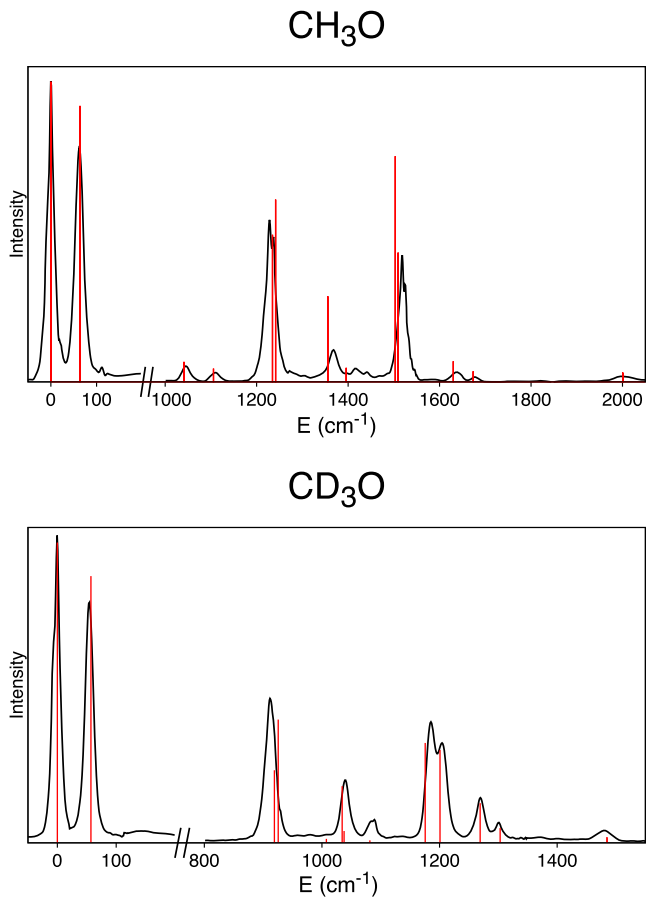

FIG. 4. Cryo-SEVI spectra of CH_3O and CD_3O (black) and simulated spectra using the KDC model Hamiltonian (red sticks). The maximum quantum number for basis functions in each mode is (5, 6, 6, 5, 5, 6, 6, 9, 9) for CH_3O and (4, 7, 7, 4, 4, 7, 7, 8, 8) for CD_3O. Spectra are plotted in cm^{-1} relative to the position of the vibrational origin at 12 654 cm^{-1} for CH_3O and 12 543 cm^{-1} for CD_3O.

thanks to the relatively high resolution of SEVI; in previous LIF and IR experiments, only one peak centered around 1650 cm^{-1} was reported for this region. The quartic Hamiltonian calculation yields two energy levels of 1630 cm^{-1} and 1674 cm^{-1}, which are in good agreement with the experimental values. Based on the calculated wave functions, we are able to assign these two levels as the spin-orbit components of the 6_2 states. This also seems consistent with the assignment of two levels of 1681 cm^{-1} and 1725 cm^{-1} to 6_2 states by Shao and Mo,[28] considering that the energy levels obtained by these authors generally lie higher in energy than the features in the SEVI spectra.

Interestingly, the a_1 components of 5_1 (1441 cm^{-1}, peak *h* in Fig. 1) and 3_16_1 (1741 cm^{-1}, peak *l* in Fig. 1) are seen in the SEVI spectrum, and the a_1 component of 6_1 (677 cm^{-1}) has also been observed by Ramond *et al.*,[23] despite the fact that these three levels are symmetry forbidden within the Condon approximation with the two-state model used here. Rather, it is the vibronic coupling between the ground electronic state and the electronically excited $\tilde{A}^2A_1$ state that gives rise to the nonzero intensities for these levels in the photoelectron spectrum. Other experiments in the literature have similarly reported evidence of vibronic coupling between electronic states of methoxy.[14,15,49] In a three-state parametrization, the wave function of a target vibronic state can be written as

$$\Psi_c = \psi^A \phi_c^A + \psi^B \phi_c^B + \psi^{A_1} \phi_c^{A_1}. \quad (12)$$

When Ψ_c is of a_1 symmetry, $\phi_c^{A_1}$ is totally symmetric and can have a nonzero overlap with the vibrational part of the anion ground state wave function ϕ_{gr}^{anion}. Therefore, the $\tilde{A}^2A_1$ electronic state is responsible for the appearance of a_1 vibronic states. In future work, it might be interesting to construct a three-state model Hamiltonian and see to what degree this affects the appearance of the spectrum. While peaks *h* and *l* in the spectrum of CH_3O have distinct vibronic symmetry from their neighbors and should therefore demonstrate distinct anisotropy, this cannot be confirmed with the current experiment as the sensitivity of the SEVI spectrometer is unfortunately not conducive to measuring the anisotropies for such weak features.

The assignment for the CH_3O vibronic energy levels between 2000 and 2500 cm^{-1} (Table VI) is significantly less straightforward due to two considerations: the quality of the vibronic energy levels calculated from the diabatic Hamiltonian degrades rapidly with increasing energy and the fact that many states in this region have significant contributions from more than one vibrational basis function. For most of the energy levels in this range, it is still possible to find one basis function that contributes more significantly than others to help assign the level. However, the two levels lying at 2199 cm^{-1} and 2222 cm^{-1} are very strongly mixed, and therefore the meaningful assignment of these states to a set of vibrational quantum numbers is probably not possible. The calculated spectrum agrees reasonably well with the experimental spectrum in this region, as shown in Fig. 5, although the agreement is less satisfactory in comparison to that for the lower levels due to the degradation in the quality of the Hamiltonian in this energy range. For example, the calculated energy levels in the range of 2300–2500 cm^{-1} appear to systematically fall roughly 20 cm^{-1} below the observed bands in the spectrum. Nevertheless, we have been able to assign a number of features in this region.

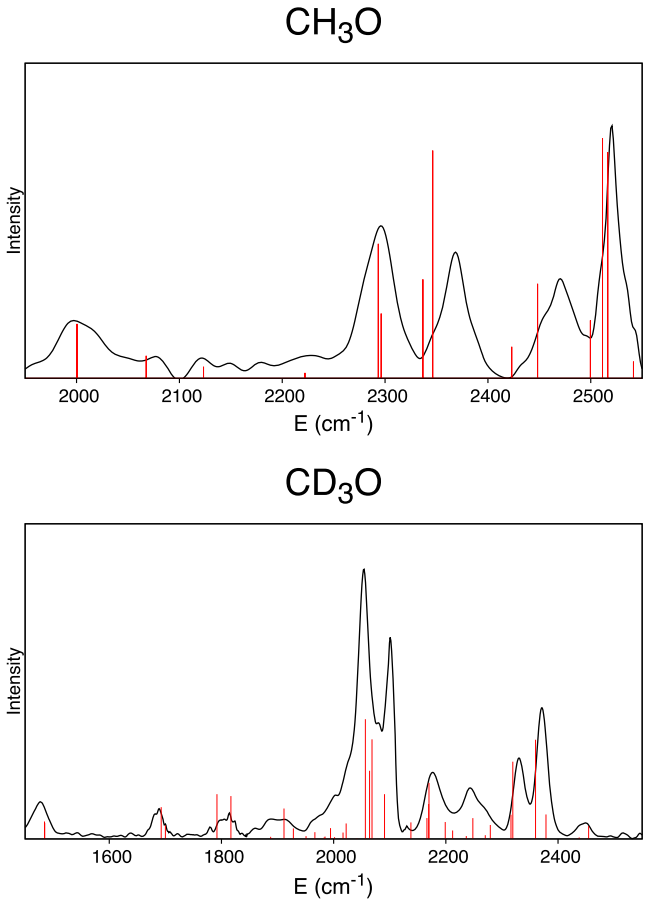

FIG. 5. Cryo-SEVI spectra of CH_3O and CD_3O (black) showing the higher-lying vibronic structure and simulated spectra using the KDC model Hamiltonian (red sticks). The maximum quantum number for basis functions in each mode is (5, 6, 6, 5, 5, 6, 6, 9, 9) for CH_3O and (4, 7, 7, 4, 4, 7, 7, 8, 8) for CD_3O. Spectra are plotted in cm^{-1} relative to the position of the vibrational origin at 12 654 cm^{-1} for CH_3O and 12 543 cm^{-1} for CD_3O.

C. Computed spectra and assignment for CD_3O

As shown in the lower half of Fig. 4, the computed spectrum for vibronic levels up to 1500 cm^{-1} agrees very well with the experimental spectrum for the perdeuterated isomer. The CD_3O cryo-SEVI level positions and their assignments are listed in Table III, while our experimental and theoretical CD_3O results are compared with those from the literature in Table V. The spectrum for CD_3O is more congested than that of CH_3O. Due to isotopic effects, modes 2, 5, and 6 (umbrella mode, scissoring mode, and rocking mode) have significantly lower frequencies in CD_3O than in CH_3O. As shown in Table III, the 2_1, 3_1, and 5_1 levels lie in the range of 1000–1200 cm^{-1}; for CH_3O, these levels span the range of 1000–1500 cm^{-1}. As mode 3 (C–O stretching) lies around 1000 cm^{-1}, modes 2, 5, and 6 in CD_3O are more significantly coupled with mode 3, which also manifests in the assignments in Table III. In the present study, the spin-orbit components of

5_1 (peaks *f* and *g* in Fig. 2) and 6_2 (peaks *h* and *i* in Fig. 2) are experimentally resolved, and the relative intensities of the spin-orbit components are consistent with calculation. The present SEVI experiment does not resolve the spin-orbit components for 6_1 (feature *c* in Fig. 2) and does not distinguish the $e_{1/2}$ component of 3_1 and the $e_{3/2}$ component of 2_1 (feature *d* in Fig. 2), which are split by less than 10 cm^{-1}.

The assignment for vibronic levels beyond 1500 cm^{-1} is again much less straightforward due to significant coupling between vibrational basis functions of various modes. In Table VI, we present the calculated $e_{1/2}$ and $e_{3/2}$ vibronic levels (which have nonzero intensities in the photoelectron spectra) in the range of 1500–2000 cm^{-1}. The assignment of these vibronic levels to meaningful quantum numbers is in general not possible; we could only find leading vibrational basis functions for a few levels in this region. The spectrum beyond 2000 cm^{-1} is even more congested and is not discussed here. However, interestingly, the calculated spectrum in the region of 1500–2500 cm^{-1} agrees quite well with the experimental data, as shown in the lower half of Fig. 5. In future work, it might be interesting to improve the resolution of photoelectron spectra in this region to resolve these vibronic levels in more detail.

D. Interplay between spin-orbit and vibronic coupling

The interplay between spin-orbit coupling and vibronic coupling, which results in the partial vibronic quenching of spin-orbit splittings in methoxy, is prototypical and of significant interest.[50] Without spin-orbit coupling, the two partners of the vibronic levels in *e* symmetry are degenerate. Recall that we work with real-valued electronic and vibrational basis functions, and the two components of *e* vibronic levels belong to a' and a'' irreducible representations in the C_s subgroup. They will, respectively, be denoted using subscripts "*a*" and "*b*" in the following discussion. In this notation, the two partners of the *e* vibronic wave functions, which are degenerate in the absence of spin-orbit coupling, can be resolved as

$$\Psi_a = \sum_{n\in A_1} c_n^{A_1}\psi_a\phi_n + \sum_{m\in E} c_m^{E}(\psi_a\phi_{m,a} - \psi_b\phi_{m,b}) + \sum_{k\in A_2} c_k^{A_2}\psi_b\phi_k, \tag{13}$$

$$\Psi_b = \sum_{n\in A_1} c_n^{A_1}\psi_b\phi_n - \sum_{m\in E} c_m^{E}(\psi_b\phi_{m,a} + \psi_a\phi_{m,b}) + \sum_{k\in A_2} c_k^{A_2}\psi_a\phi_k, \tag{14}$$

where $\{\phi_n\}$, $\{\phi_m\}$, and $\{\phi_k\}$ represent the set of vibrational basis functions of irreducible representations A_1, E, and A_2, respectively. For example, the vibrational basis function for the totally symmetric C–O stretching mode ϕ_{3_1} belongs to $\{\phi_n\}$, and the vibrational basis functions $\phi_{6_1,a}$ and $\phi_{6_1,b}$ for the rocking mode, which is Jahn-Teller active, belong to $\{\phi_{m,a}\}$ and $\{\phi_{m,b}\}$. An example for a function in $\{\phi_k\}$ is the combination of the products of functions in *e* symmetry: $\phi_{6_1,a}\phi_{5_1,b} - \phi_{6_1,b}\phi_{5_1,a}$. We base our following discussions mainly on numerical results of CH_3O, as the conclusions also hold for CD_3O.

Using Eqs. (13) and (14), the spin-orbit coupling matrix elements between the two degenerate vibronic states $\langle\Psi_a|\hat{h}_{SO}|\Psi_b\rangle$ can be reduced to the corresponding electronic spin-orbit matrix elements weighted by a linear combination of the square of the coefficients

$$\langle\Psi_a|\hat{h}_{SO}|\Psi_b\rangle = \langle\psi_a|\hat{h}_{SO}|\psi_b\rangle\Big(\sum_{n\in A_1}(c_n^{A_1})^2 - \sum_{m\in E}2(c_m^{E})^2 - \sum_{k\in A_2}(c_k^{A_2})^2\Big). \tag{15}$$

A close inspection of Eq. (15) shows that $|\sum_{n\in A_1}(c_n^{A_1})^2 - \sum_{m\in E}2(c_m^{E})^2 - \sum_{k\in A_2}(c_k^{A_2})^2|$ is nothing but the quenching factor for spin-orbit splitting. For example, the vibronic wave functions for the origin band of CH_3O mainly consist of 0_0 and the Jahn-Teller mode 6_1 with $c_{0_0} \approx 0.82$ and $c_{6_1} \approx 0.32$. Basing a simple analysis on these two coefficients only, one obtains a quenching factor of approximately 0.47. Combining

TABLE VI. Computed $e_{1/2}$ and $e_{3/2}$ vibronic levels from 2000 to 2500 cm^{-1} above the vibrational origin in the ground electronic state of CH_3O and from 1500 to 2000 cm^{-1} in the ground electronic state of CD_3O.

CH_3O					CD_3O				
Level	Symmetry	Reference 28	Reference 12	Present	Level	Symmetry	Reference 28	Reference 12	Present
3_2	$e_{3/2}$	2078	2074	2068	...	$e_{1/2}$	1715	1679	1693
3_2	$e_{1/2}$	2139	2130	2124	...	$e_{3/2}$	1716	1689	1700
...	$e_{1/2}$	2251	2186	2199	...	$e_{1/2}$	1818	1792	1792
...	$e_{3/2}$	2274	2208	2222	...	$e_{3/2}$	1867	...	1817
$5_1 6_1$	$e_{1/2}$	2334	2292	2293	...	$e_{1/2}$	1912	1883	1888
$5_1 6_1$	$e_{3/2}$	2345	2299	2296	...	$e_{3/2}$	1914	1895	1891
$3_1 5_1$	$e_{1/2}$	2390	2362	2337	...	$e_{3/2}$	1923	...	1912
$3_1 5_1$	$e_{3/2}$	2397	2373	2347	...	$e_{1/2}$	1927	...	1928
$2_1 3_1$	$e_{3/2}$	2430	2449	2423	...	$e_{3/2}$	1940	1958	1951
...	$e_{1/2}$	2486	2466	2448	...	$e_{1/2}$	1989	1959	1967
...	$e_{3/2}$	2531	2514	2500	...	$e_{1/2}$	1992	1974	1983
$2_1 3_1$	$e_{1/2}$	2504	2528	2512	3_2	$e_{3/2}$	1996	...	1985
...	$e_{3/2}$	2508	2529	2517	1_1	$e_{3/2}$	2005	2010	2002

this quenching factor with the value of -133 cm^{-1} calculated for the spin-orbit matrix elements between diabatic electronic wave functions, the spin-orbit splitting for the origin band can be estimated as 63 cm^{-1}, which compares favorably with the experimental value 62 cm^{-1} (as well as the value of 64 cm^{-1} obtained from full-fledged calculations).

Further, Eq. (15) also implies that, when the vibronic state is dominated by totally symmetric vibrational functions ($\sum_{n\in A_1}(c_n^{A_1})^2 > 2\sum_{m\in E}(c_m^E)^2 + \sum_{k\in E}(c_k^{A_2})^2$), the spin-orbit interaction constant for the vibronic state has the same sign as the electronic spin-orbit interaction constant. As the electronic spin-orbit coupling constant of methoxy takes a negative value, the $e_{3/2}$ levels are lower than the corresponding $e_{1/2}$ levels. This is shown in Table II to hold for all the low-lying symmetric modes of CH_3O, 0_0, 3_1, and 2_1. In contrast, for those vibronic states dominated by vibrational functions of E symmetry, the sign given by Eq. (13) is reversed. Therefore, the $e_{1/2}$ levels of such states lie lower than the corresponding $e_{3/2}$ levels, as is true, for example, for the 6_1 and 5_1 states. We note that there are substantial mixtures of 0_0 in the wave function of 6_1 states and of 2_1 in the wave functions of 5_1 states. Consequently, the spin-orbit splittings in these two cases are very small (7 cm^{-1} for 6_1 and 6 cm^{-1} for 5_1) due to a near cancellation between $\sum_{n\in A_1}(c_n^{A_1})^2$ and $2\sum_{m\in E}(c_m^E)^2$ in the expression of the quenching factor.

E. Relative intensities for the spin-orbit components

The relative magnitude of intensities for the spin-orbit components ($e_{1/2}$ and $e_{3/2}$) in CH_3O is an interesting topic that also warrants additional discussion. In a perturbative picture, in which spin-orbit coupling is considered up to leading order within degenerate perturbation theory, the intensities for the two spin-orbit components are identical. Therefore, the difference between the intensities of two spin-orbit partners is a higher-order effect and comes from the different coupling of the two spin-orbit partners with other scalar vibronic wave functions due to spin-orbit coupling. Such a higher-order effect is negligible for low-lying vibronic states as they are well separated from other states; the difference between the intensities of the two spin-orbit components is relatively small (within 20% of the total intensity) for 0_0, 3_1, and 6_1. However, coupling with other scalar vibronic wave functions can be significant for higher vibronic levels. For example, the $e_{1/2}$ component of the 2_1 level receives substantially more contribution from 5_1 basis functions than the corresponding $e_{3/2}$ component. Consequently, the difference between the intensities for the spin-orbit components is larger; the intensity for the $e_{1/2}$ component of the 2_1 state is more than twice that of the $e_{3/2}$ component. Among the six spin-orbit pairs (0_0, 6_1, 3_1, 2_1, 5_1, and 6_2) that reside within 2000 cm^{-1} of the origin (with energies of 0/62, 1045/1110, 1228/1237, 1368/1416, 1518/1527, and 1638/1677 cm^{-1}, respectively), the calculated intensity ratios are quite similar to those seen in the experiment, which is a testament to the good quality of the vibronic Hamiltonian. The only qualitative disagreement that can be found occurs for the 6_1 level, where the calculated intensity for the (lower-energy) $e_{1/2}$ component is a bit larger than for the $e_{3/2}$ sublevel. In the SEVI spectrum, taken at an energy just slightly above this pair so as to resolve the doublet, the situation is reversed: the lower-energy feature has a slightly greater intensity. However, as this is taken quite close to threshold, the intensities of these two features are subject to important threshold effects of the photodetachment cross section.[51] Given how close both the observed and calculated intensities are to each other, it is really not meaningful to draw any conclusions from this observation. Indeed, SEVI spectra taken at higher energies, which are insufficient to resolve the spin-orbit pair, exhibit a small asymmetry of this feature in the direction that is consistent with the calculated intensities. A more careful analysis based on computed photodetachment cross sections would be interesting here. It might also be illuminating to see how the vibronic coupling between the electronic ground state and the $\tilde{A}^2A_1$ state and/or the inclusion of higher order force fields affects these intensities.

IV. SUMMARY

The low-lying vibronic level structure of the ground state of methoxy (vibronic levels up to 2000 cm^{-1} above the vibrational origin for CH_3O and up to 1500 cm^{-1} for CD_3O) is now fully understood, with the aid of cryo-SEVI spectra combined with Köppel-Domcke-Cederbaum (KDC) vibronic Hamiltonian calculations. The high-resolution cryo-SEVI technique yields refined electron affinities for CH_3O and CD_3O and resolves narrow splittings not seen in previous photoelectron experiments. The accompanying calculations accurately capture subtle features of the experimental spectra, including distinct spin-orbit splitting magnitudes for different vibrational states, and the relative intensities of spin-orbit components. Signals of a_1 vibronic levels observed in cryo-SEVI spectra also provide the direct evidence of vibronic coupling between the ground state and the electronically excited $\tilde{A}^2A_1$ state. Future computational studies might include the construction of a three-state model Hamiltonian that is capable of capturing such effects. Contributions from quintic and sextic force constants as well as the geometrical dependence of spin-orbit coupling constants might be considered to further enhance the computational accuracy. Future experimental work could better resolve the higher-lying vibronic structure for CH_3O and CD_3O.

ACKNOWLEDGMENTS

The work was supported by the Director, Office of Basic Energy Sciences, Chemical Sciences Division of the U.S. Department of Energy under Contract Nos. DE-AC02-05CH11231 (M.L.W., J.B.K., and D.M.N.) and DE-FG02-07ER15884 (J.F.S.) and the National Science Foundation under Grant No. CHE-1361031 (L.C. and J.F.S.). M.L.W. thanks the National Science Foundation for a graduate research fellowship.

[1] K. L. Demerjian, J. A. Kerr, and J. G. Calvert, Adv. Environ. Sci. Technol. **4**, 1 (1974).
[2] W. A. Glasson, Environ. Sci. Technol. **9**, 1048 (1975).
[3] R. Zellner, B. Fritz, and K. Lorenz, J. Atmos. Chem. **4**, 241 (1986).

[4]J. G. Calvert, R. G. Derwent, J. J. Orlando, G. S. Tyndall, and T. J. Wallington, *Mechanisms of Atmospheric Oxidation of the Alkanes* (Oxford, New York, 2008).
[5]D. Hucknall, *Chemistry of Hydrocarbon Combustion* (Springer, Berlin, 2009).
[6]J. A. Wargon and F. Williams, J. Am. Chem. Soc. **94**, 7917 (1972).
[7]See, for example, J. K. N. Wan, in *Advances in Photochemistry*, edited by J. N. Pitts, G. S. Hammon, and K. Gollnick (Wiley, New York, 2009), Vol. 9, pp. 1–146.
[8]D. R. Yarkony, H. F. Schaefer, and S. Rothenburg, J. Am. Chem. Soc. **96**, 656 (1974).
[9]J. Liu and T. A. Miller, J. Phys. Chem. A **118**, 11871 (2014).
[10]D. W. G. Style and J. C. Ward, Trans. Faraday Soc. **49**, 999 (1953).
[11]Here and elsewhere in this paper, the "ground state" is taken to refer to the doubly degenerate ^2E state, which is really two states.
[12]Y.-F. Lee, W.-T. Chou, B. A. Johnson, D. P. Tabor, and E. L. Sibert, J. Mol. Spectrosc. **310**, 57 (2015).
[13]D. L. Osborn, D. J. Leahy, and D. M. Neumark, J. Phys. Chem. A **101**, 6583 (1997).
[14]A. Geers, J. Kappert, F. Temps, and T. Sears, J. Chem. Phys. **98**, 4297 (1993).
[15]A. Geers, J. Kappert, F. Temps, and J. W. Wiebrecht, J. Chem. Phys. **101**, 3618 (1994).
[16]S. C. Foster, P. Misra, T.-Y. D. Lin, C. P. Damo, C. C. Carter, and T. A. Miller, J. Phys. Chem. **92**, 5914 (1988).
[17]J. Liu, M.-W. Chen, D. Melnik, J. T. Yi, and T. A. Miller, J. Chem. Phys. **130**, 074302 (2009).
[18]J. Liu, M.-W. Chen, D. Melnik, T. A. Miller, Y. Endo, and E. Hirota, J. Chem. Phys. **130**, 074303 (2009).
[19]Y.-Y. Lee, G.-H. Wann, and Y.-P. Lee, J. Chem. Phys. **99**, 9465 (1993).
[20]P. Misra, X. Zhu, C.-Y. Hsueh, and J. B. Halpern, Chem. Phys. **178**, 377 (1993).
[21]P. C. Engelking, G. B. Ellison, and W. C. Lineberger, J. Chem. Phys. **69**, 1826 (1978).
[22]D. L. Osborn, D. J. Leahy, E. H. Kim, E. de Beer, and D. M. Neumark, Chem. Phys. Lett. **292**, 651 (1998).
[23]T. M. Ramond, G. E. Davico, R. L. Schwartz, and W. C. Lineberger, J. Chem. Phys. **112**, 1158 (2000).
[24]D. M. Neumark, J. Phys. Chem. A **112**, 13287 (2008).
[25]M. J. Nee, A. Osterwalder, J. Zhou, and D. M. Neumark, J. Chem. Phys. **125**, 014306 (2006).
[26]U. Höpper, P. Botschwina, and H. Köppel, J. Chem. Phys. **112**, 4132 (2000).
[27]A. V. Marenich and J. E. Boggs, J. Chem. Phys. **122**, 024308 (2005).
[28]Z. Shao and Y. Mo, J. Chem. Phys. **138**, 244309 (2013).
[29]H. Köppel, W. Domcke, and L. S. Cederbaum, Adv. Chem. Phys. **57**, 59 (1984).
[30]T. Pacher, L. S. Cederbaum, and H. Köppel, Adv. Chem. Phys. **84**, 293 (1993).
[31]K. Raghavachari, G. W. Trucks, J. A. Pople, and M. Head-Gordon, Chem. Phys. Lett. **157**, 479 (1989).
[32]T. H. Dunning, J. Chem. Phys. **90**, 1007 (1989).
[33]C. Hock, J. B. Kim, M. L. Weichman, T. L. Yacovitch, and D. M. Neumark, J. Chem. Phys. **137**, 244201 (2012).
[34]M. L. Weichman, J. A. DeVine, D. S. Levine, J. B. Kim, and D. M. Neumark, Proc. Natl. Acad. Sci. U. S. A. **113**, 1698 (2016).
[35]U. Even, J. Jortner, D. Noy, N. Lavie, and C. Cossart-Magos, J. Chem. Phys. **112**, 8068 (2000).
[36]A. T. J. B. Eppink and D. H. Parker, Rev. Sci. Instrum. **68**, 3477 (1997).
[37]D. W. Chandler and P. L. Houston, J. Chem. Phys. **87**, 1445 (1987).
[38]M. B. Doyle, C. Abeyasera, and A. G. Suits, NuACQ, http://chem.wayne.edu/suitsgroup/NuACQ.html.
[39]B. Dick, Phys. Chem. Chem. Phys. **16**, 570 (2014).
[40]C. Blondel, W. Chaibi, C. Delsart, C. Drag, F. Goldfarb, and S. Kröger, Eur. Phys. J. D **33**, 335 (2005).
[41]J. F. Stanton and J. Gauss, J. Chem. Phys. **101**, 8938 (1994).
[42]J. Almlöf and P. R. Taylor, J. Chem. Phys. **86**, 4070 (1987).
[43]For a review, see R. J. Bartlett and M. Musial, Rev. Mod. Phys. **79**, 291 (2007).
[44]K. Klein and J. Gauss, J. Chem. Phys. **129**, 194106 (2008).
[45]F. Neese, J. Chem. Phys. **122**, 034107 (2005).
[46]R. Mabbs, E. R. Grumbling, K. Pichugin, and A. Sanov, Chem. Soc. Rev. **38**, 2169 (2009).
[47]C. S. Simmons, T. Ichino, and J. F. Stanton, J. Phys. Chem. Lett. **3**, 1946 (2012).
[48]K. Klein, E. Garand, T. Ichino, D. M. Neumark, J. Gauss, and J. F. Stanton, Theor. Chem. Acc. **129**, 527 (2011).
[49]D. E. Powers, M. B. Pushkarsky, and T. A. Miller, J. Chem. Phys. **106**, 6863 (1997).
[50]T. A. Barckholtz and T. A. Miller, Int. Rev. Phys. Chem. **17**, 435 (1998), and references therein.
[51]E. P. Wigner, Phys. Rev. **73**, 1002 (1948).